Cell Research

www.nature.com/cr
www.cell-research.com

LETTER TO THE EDITOR

Cryo-EM structures of human pannexin 1 channel

Cell Research (2020) 30:449–451; https://doi.org/10.1038/s41422-020-0310-0

Dear Editor,

Pannexin 1 (PANX1) channel mediates adenosine-5′-triphosphate (ATP) release for purinergic signaling,[1] playing important roles in multiple physiological and pathological processes including apoptotic clearance,[2] inflammatory response,[3] cancer progression, and metastasis.[4] Diverse stimuli have been reported to activate PANX1 channel, such as voltage, membrane stretch, hypotonicity, elevated extracellular K^+ or intracellular Ca^{2+} concentration, C-terminal cleavage and phosphorylation.[1,5] It is perplexing that PANX1 has been demonstrated to exhibit different unitary channel properties depending on the mode of activation.[1,5] Particularly, PANX1 undergoes a stepwise, quantized activation progress upon sequentially cleaving the C-terminal of each subunit.[6]

We tested PANX1 channel activation by C-terminal cleavage, hypotonicity, and elevation in extracellular K^+ concentration in human embryonic kidney (HEK)-293T cells through an ATP releasing assay. The detailed procedure is described in Supplementary information, Data S1. ATP concentration only significantly rises in supernatants from cells transfected with a truncated form of human PANX1 (designated as $PANX1_{\Delta C}$, with D376–S426 truncated to mimic a caspase-cleaved form of PANX1[7,8]). This signal is remarkably eliminated upon pre-incubation of the cells with carbenoxolone (CBX), a well-known PANX1 inhibitor[9] (Supplementary information, Fig. S1a). This observation is in accordance with previous demonstration of PANX1 channel activation by apoptosis-induced C-terminal cleavage by caspase.[7] By contrast, no significant differences of ATP concentration were found upon exposure to buffers of either high K^+ concentration or low ionic strength, consistent with previously observation that high extracellular K^+-induced PANX1 current or dye uptake were not verified,[5] indicating that the two activation mechanisms are not applicable in HEK293T cells (Supplementary information, Fig. S1b and c). We then mainly focused on the C-terminal cleavage-based activation mechanism in this study.

To structurally explicate the activation mechanism, we designed, expressed and purified three different hPANX1s, a full-length wild-type hPANX1 (designated as $PANX1_{WT}$), $PANX1_{\Delta C,}$ and a double mutated hPANX1 (designated as $PANX1_{EE}$, with D376E/D379E double mutation to eliminate the caspase-cleavage site) (Supplementary information, Fig. S3a–d). However, we were unable to purify enough $PANX1_{\Delta C}$ for structural study since cells expressing $PANX1_{\Delta C}$ became sick and stopped growing. The purified $PANX1_{WT}$ exhibits two bands near a relative molecular mass of 45,000 (M_r 45 kD) and a higher band on SDS-polyacrylamide gel electrophoresis (PAGE), corresponding to the three glycosylation states of full-length PANX1 as mentioned in previous study[10] (Supplementary information, Fig. S2b). However, we unexpectedly observed an additional band near a relative molecular mass of 38,000 (M_r 38 kD) (Supplementary information, Figs. S2b and S3b). Mass spectrometry shows that the roughly 38 kD band contains a truncated form with Lys374 being the last detectable amino acid. The following motif $_{376}$DVVD$_{379}$ was reported to be recognized and cleaved by caspase,[7] indicating a partial C-terminal caspase cleavage of $PANX1_{WT}$ (Supplementary information, Fig. S2a). Mutation of the caspase-cleavage site eliminated the 38 kD product (Supplementary information, Fig. S3d). In addition, we also purified $PANX1_{EE}$ in the presence of CBX (designated as $PANX1_{CBX}$) to study the CBX inhibition mechanism (Supplementary information, Fig. S3e and f).

We determined the cryo-EM structures of $PANX1_{WT}$, $PANX1_{EE}$, and $PANX1_{CBX}$ to an overall resolution of 4.1 Å, 3.6 Å, and 4.6 Å, respectively (Fig. 1a; Supplementary information, Table S1). The three EM datasets were processed following the same procedure (Supplementary information, Figs. S4–S6). The EM density of $PANX1_{EE}$ showed well-resolved extracellular domain (ECD) and transmembrane domain (TMD) with clearly visible α-helical features and densities for bulky amino-acid side chains, and was sufficient for de novo model building (Fig. 1b; Supplementary information, Fig. S8a). The model of $PANX1_{EE}$ was further docked in and refined against the maps of $PANX1_{WT}$ and $PANX1_{CBX}$ (Supplementary information, Figs. S8b and S9). Despite a hexameric assembly of PANX1 was reported by several studies,[6,10,11] All the three structures reveal a heptameric assembly (Fig. 1c; Supplementary information, Fig. S9b and d). To confirm the oligomeric statement of PANX1 in a more native condition, we determined the structure of $PANX1_{WT}$ reconstituted into lipid nanodiscs (designated as $PANX1_{ND}$) (Supplementary information, Table S1, Figs. S3g, h and S7). Albeit with low resolution, it clearly displays a heptameric assembly (Supplementary information, Fig. S7e).

The overall structure of PANX1 adopts a conical shape in the view parallel to membrane. The heptameric channel is ~105 Å long and ~100 Å wide, with flat ECD protruding ~35 Å above cell membrane and intracellular domain (ICD) extending ~35 Å to cytoplasm (Fig. 1b). Each subunit resembles that of a typical large pore-forming channels despite the lack of sequence identity (Fig. 1d, e; Supplementary information, Figs. S10 and S11a, b). A PANX1 protomer contains four transmembrane helices (TM1–TM4) connected by two extracellular linkers (EL1 and EL2) and an intracellular linker (IL). EL1 contains an alpha-helix (E1H) and a short beta-strand (E1β) in parallel facing towards center pore; EL2 contains two antiparallel beta-strands (E2β1 and E2β2) connected by a glycosylated loop embracing EL1. The two ELs are stabilized by two conserved inter-chain disulfate bonds formed by Cys66-Cys265 and Cys84-Cys246 (Supplementary information, Fig. S11c–e). The seven EL1s pack consecutively and tightly with several inter-subunit polar interactions observed, including Tyr83-Lys266, Gln90-Lys266, Gln90-Glu243, and Arg254-Gln264 (Fig. 1f). IL contains two alpha-helices (IH1 and IH2) and a disordered region of 38 residues (Lys157–Pro194). Both termini of the protein are at intracellular side facing the channel center, in which N-terminal region (M1–V34) is short and completely invisible in the structure while C-terminal (CT) domain contains two alpha-helices (CH1 and CH2) assigned and a long missing tail consisting of 90 residues (E337–C426).

The substrate conduction path of PANX1 is along the central axis constituted mainly by E1H, TM1 and IH1 (Fig. 1g). The channel pore exhibits two apparent constrictions both harbored at extracellular side (Fig. 1h). Trp74 on E1H forms the narrowest part of the channel with a diameter of 9.4 Å, which is wide enough for the passage of

Received: 17 January 2020 Accepted: 15 March 2020
Published online: 3 April 2020

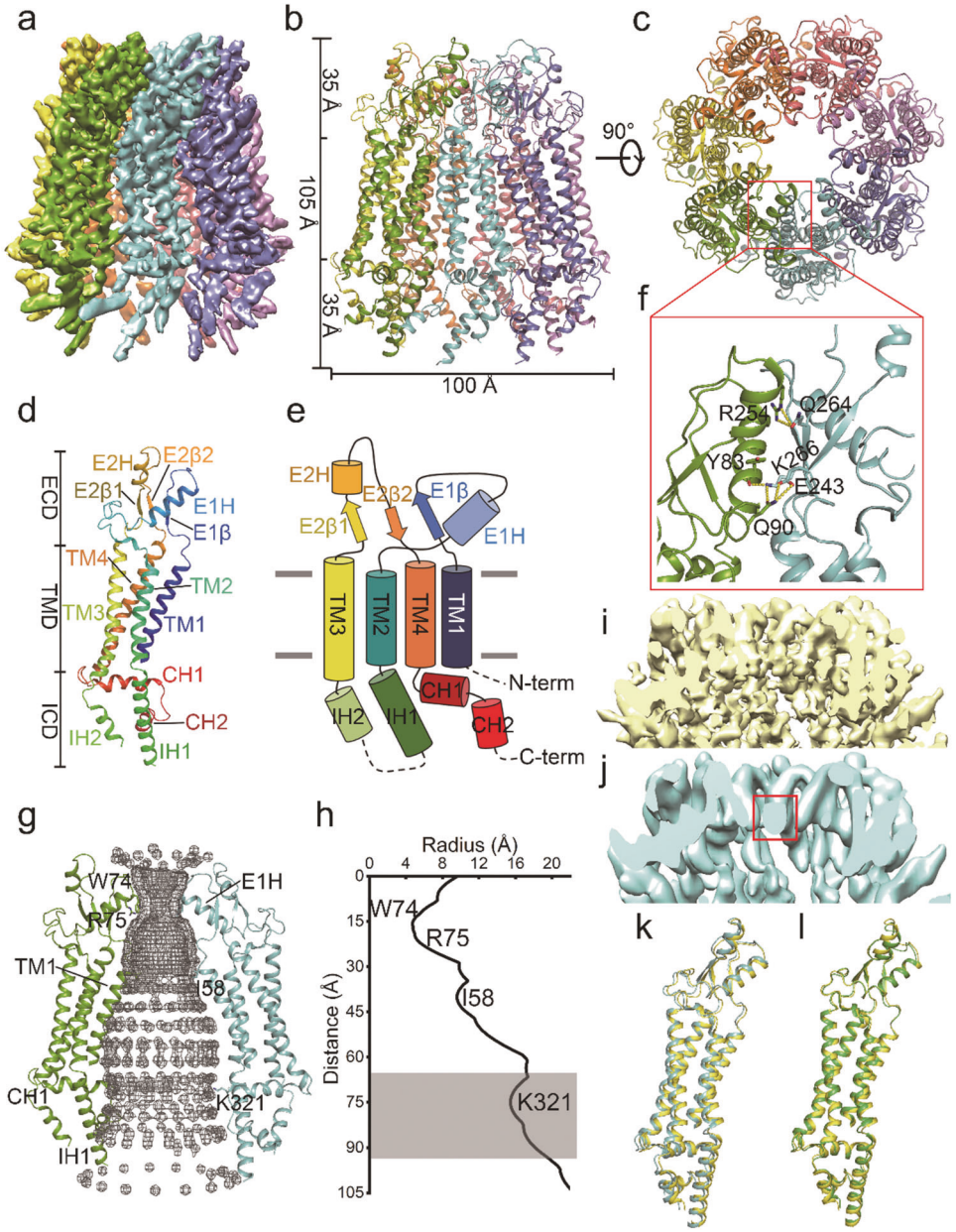

Fig. 1 Cryo-EM structure of human Pannexin 1 (PANX1) channel. a The Cryo-EM density map of $PANX1_{EE}$ viewed parallel to the plasma membrane. **b**, **c** Ribbon representations of the heptameric structure of $PANX1_{EE}$ viewed parallel to the plasma membrane (**b**) or from the extracellular side down the sevenfold symmetry axis (**c**). **d** Ribbon representation of the protomer structure of $PANX1_{EE}$. **e** Schematic representation of the PANX1 topology. Gray lines indicate the estimated lipid bilayer borders. **f** A zoom in view of the subunits interface with interactions labeled. **g** Ribbon representation of the channel pore with the substrate conduction pathway displayed in gray mesh. Key domains and residues are labeled. **h** The pore radius along the substrate conduction pathway calculated by HOLE program.[14] Residues forming the constrictions are labeled. **i**, **j** The Cryo-EM density maps of the extracellular gate in $PANX1_{EE}$ (**i**) or $PANX1_{CBX}$ (**j**). The density corresponding to CBX is highlighted in red box. **k** Representation of single subunit of a superimposed overall structure of $PANX1_{EE}$ (yellow) and $PANX1_{CBX}$ (cyan). **l** Representation of single subunit of a superimposed overall structure of $PANX1_{EE}$ (yellow) and $PANX1_{WT}$ (green).

large molecules including ATP (Supplementary information, Fig. S12b and e); Ile58, the ending residue of TM1, forms the second constriction with a diameter of 19.2 Å (Supplementary information, Fig. S12c and f). In the membrane encapsulated segment, the channel pore is gradually broadened to the intracellular side due to the tilted TM1 and the widened pore is maintained at ICD (Supplementary information, Fig. S12d and g). Several investigations manifested that the C-terminus of PANX1 serves as an auto-inhibitory domain participating channel pore.[8] Also, N-terminus of PANX1 is likely situated in the pore according to structural comparisons (Supplementary information, Fig. S11a). As a consequence, the dimensions of ICD of substrate permeable pathway are not accurately defined and we will not discuss at present work (Fig. 1h). Most residues exposed to the substrate pathway are uncharged, with an exception of Arg75 which locates nearby Trp74 pointing towards center pore and may contribute to the anion-selectivity of positive membrane potential activated PANX1 channel[12] (Supplementary information, Fig. S12a–c).

Comparing to the map of $PANX1_{EE}$, the map of $PANX1_{CBX}$ reveals an additional density plugging at the top of the center pore within the Trp74 ring (Fig. 1i, j). Two lines of evidence support that the barrel-shaped density is corresponding to CBX.

First, comparing to $PANX1_{EE}$, the only additional chemical component in $PANX1_{CBX}$ is CBX. Second, Trp74 has been observed to be directly involved in CBX-mediated PANX1 inhibition. Mutation of Trp74 to any other residues except phenylalanine eliminates the activity of CBX.[9] Due to the sevenfold averaging, the information of the exact location and orientation of CBX is missing. However, based on the chemical structures of CBX and surrounded residues, it is suggested that hydrophobic interactions between naphthyl group and indole rings mainly contribute to the CBX binding. No detectable conformational change has been observed between PANX1 structures with or without CBX (Fig. 1k), suggesting a simple inhibition mechanism whereby CBX rigidly plugs in the extracellular gate of PANX1 and thus blocks the substrate conduction. Such a 'cork-in-bottle' pattern has also been reported in the inhibition mechanism of VRAC by DCPIB.[13]

By comparing the structures of $PANX1_{EE}$ and $PANX1_{WT}$ that corresponding to the conformations of PANX1 with intact C-termini and with partial C-termini cleaved, a slightly expanded pore radius at the interface of TMD and ICD is observed due to the rearrangement of ICD while the overall architecture is virtually identical (Fig. 1l; Supplementary information, Fig. S13), indicating that the activation by C-terminal cleavage do not induce a whole conformational change of the pore forming domains and supporting the hypothesis that C-terminal serves as a cytoplasmic blocker.[8] However, we are not able to provide the description of the individual movements of a subunit upon C-terminal cleavage due to the following two reasons. First, on account of the C7 symmetry imposed during the structure determination, $PANX1_{WT}$ represents an averaged architecture of full length subunits and C-terminal truncated subunits. Second, the local resolution of the cytoplasmic domain is relatively low because of its mobility. To achieve a better understanding of structural activation mechanism, $PANX1_{WT}$ model without symmetry imposition at near atomic resolution and structure of $PANX1_{\Delta C}$ are required.

In summary, we determined the structures of human PANX1 channel with intact C-termini, with partial C-terminal cleavage, or in the CBX-bound inhibited state. The general structure shows a heptameric assembly with each protomer featuring a topology similar to large-pore forming channels. The comparisons of PANX1 in different states reveal that CBX rigidly plugs in the extracellular pore, thus sterically blocking substrate passage while C-terminal cleavage removes the auto-inhibitory without inducing an overall conformational change. These findings provide significant insights into the understanding of the mechanistic mechanism of PANX1 activation and inhibition.

Structure coordinates and cryo-EM density maps of $PANX1_{WT}$, $PANX1_{EE}$, $PANX1_{CBX}$ have been deposited in the protein data bank under accession number 6M66, 6M67, 6M68 and EMD-30114, EMD-30115, EMD-30116, respectively.

ACKNOWLEDGEMENTS

We acknowledge the use of Cryo-EM instruments and computing resources in Center of Cryo-Electron Microscopy, Zhejiang University, the Cryo-EM Platform of Peking University and the Cryo-EM Facility Center of Southern University of Science and Technology. This work was supported in part by Ministry of Science and Technology (2016YFA0500404 to S.Y., 2018YFA0508100 to J.G., 2016YFA0501102 to X.Z., and 2016YFA0500700 to N.G), the National Natural Science Foundation of China (31525001 and 31971127 to S.Y, 31870724 to J.G., 31600606 to X.Z., 31725007 and 31630087 to N.G., and 31700655 to N.L.), Zhejiang Provincial Natural Science Foundation (LR19C050002 to J.G), and the Fundamental Research Funds for the Central Universities (to S.Y., J.G., X.Z., and N.G.).

AUTHOR CONTRIBUTIONS

Q.J., B.Z. and S.Y. conceived the project. Q.J. and X.Z. performed molecular cloning and protein purification. Q.J., B.Z., X.Z, L.X., X.Z. and J.G. performed Cryo-EM structural analysis. Q.J., B.Z., F.S. and Y.X. performed functional studies. All authors contributed to data analysis. Q.J., J.G. and S.Y. wrote the paper.

ADDITIONAL INFORMATION

Supplementary information accompanies this paper at https://doi.org/10.1038/s41422-020-0310-0.

Competing interests: The authors declare no competing interests.

Qiuheng Jin[1], Bo Zhang[1], Xiang Zheng[2], Ningning Li[3], Lingyi Xu[4,5], Yuan Xie[4,5], Fangjun Song[4,5], Eijaz Ahmed Bhat[1], Yuan Chen[2], Ning Gao[3], Jiangtao Guo[4,5], Xiaokang Zhang[6] and Sheng Ye[1,6]

[1]Life Sciences Institute, Zhejiang University, Hangzhou, Zhejiang 310058, China; [2]The State Key Laboratory of Subtropical Silviculture, Zhejiang A & F University, 666 Wusu street, Hangzhou, Zhejiang 311300, China; [3]State Key Laboratory of Membrane Biology, Peking-Tsinghua Center for Life Sciences, School of Life Sciences, Peking University, Beijing, China; [4]Department of Biophysics, Department of Pathology of Sir Run Run Shaw Hospital, Zhejiang University School of Medicine, Hangzhou, Zhejiang 310058, China; [5]Department of Biophysics, Institute of Neuroscience, NHC and CAMS Key Laboratory of Medical Neurobiology, Zhejiang University School of Medicine, Hangzhou, Zhejiang 310058, China and [6]Tianjin Key Laboratory of Function and Application of Biological Macromolecular Structures, School of Life Sciences, Tianjin University, 92 Weijin Road, Nankai District, Tianjin 300072, China

These authors contributed equally: Qiuheng Jin, Bo Zhang, Xiang Zheng, Ningning Li

Correspondence: Jiangtao Guo (jiangtaoguo@zju.edu.cn) or Xiaokang Zhang (inter1965@qq.com) or Sheng Ye (sye@tju.edu.cn)

REFERENCES

1. Dahl, G. *Philos. Trans. R. Soc. B.* **370**, https://doi.org/10.1098/rstb.2014.0191 (2015).
2. Poon, I. K. H., Lucas, C. D., Rossi, A. G. & Ravichandran, K. S. *Nat. Rev. Immunol.* **14**, 166–180 (2014).
3. Idzko, M., Ferrari, D. & Eltzschig, H. K. *Nature* **509**, 310–317 (2014).
4. Di Virgilio, F. et al. *Nat. Rev. Cancer* **18**, 601–618 (2018).
5. Chiu, Y. H., Schappe, M. S., Desai, B. N. & Bayliss, D. A. *J. Gen. Physiol.* **150**, 19–39 (2018).
6. Chiu, Y. H. et al. *Nat. Commun.* **8**, 14324 (2017).
7. Chekeni, F. B. et al. *Nature* **467**, 863–867 (2010).
8. Sandilos, J. K. et al. *J. Biol. Chem.* **287**, 11303–11311 (2012).
9. Michalski, K. & Kawate, T. *J. Gen. Physiol.* **147**, 165–174 (2016).
10. Boassa, D. et al. *J. Biol. Chem.* **282**, 31733–31743 (2007).
11. Wang, J. et al. *Sci. Signal.* **7**, https://doi.org/10.1126/scisignal.2005431 (2014).
12. Ma, W. et al. *Pflugers Arch.* **463**, 585–592 (2012).
13. Kern, D. M., Oh, S., Hite, R. K. & Brohawn, S. G. *Elife* **8**, https://doi.org/10.7554/eLife.42636 (2019).
14. Smart, O. S. et al. *J. Mol. Gr.* **14**, 354–360, 376 (1996).